

Magnetic field-induced phases in a model $S = 1$ Haldane chain system

Ivan Jakovac  ¹ Mihael S. Grbić  ^{1,*} Maxime Dupont  ^{2,3} Nicolas Laflorencie  ² Sylvain Capponi  ² Yuko Hosokoshi  ^{4,5} Steffen Krämer  ⁶ Yurii Skourski  ⁷ Sven Luther, ⁷ Mashashi Takigawa ⁸ and Mladen Horvatić ⁶

¹Department of Physics, Faculty of Science, University of Zagreb, Bijenička cesta 32, 10000 Zagreb, Croatia

²Laboratoire de Physique Théorique, Université Paul Sabatier,

118 Route de Narbonne, 31062 Toulouse Cedex 4, France

³Present address: Rigetti Computing, 775 Heinz Avenue, Berkeley, California 94710, USA

⁴Department of Physics, Osaka Metropolitan University, Osaka, Japan

⁵Department of Physical Science, Osaka Prefecture University, Osaka, Japan

⁶Laboratoire National des Champs Magnétiques Intenses, LNCMI-CNRS (UPR3228), EMFL, Université Grenoble Alpes, Université Toulouse, INSA-T, 38042 Grenoble Cedex 9, France

⁷Hochfeld-Magnetlabor Dresden (HLD-EMFL) Helmholtz-Zentrum Dresden-Rossendorf, 01328 Dresden, Germany

⁸Institute for Solid State Physics, University of Tokyo,

5-1-5 Kashiwanoha, Kashiwa, Chiba 277-8581, Japan

(Dated: January 16, 2026)

An $S = 1$ Haldane chain is a one-dimensional (1D) quantum magnet where strong fluctuations result in quantum disordered singlet ground state with a gapped excitation spectrum. The gap magnitude is primarily set by the dominant intrachain interaction (J_{1D}). An applied magnetic field closes the gap at B_{c1} and drives the system into a gapless Tomonaga-Luttinger liquid (TLL) regime, followed by, at lower temperatures, a Bose-Einstein condensate (BEC) ground state, persisting up to $B_{c2} \propto 4J_{1D}/g\mu_B$. Almost all previously studied experimental realizations of such systems were based on transition-metal complexes which typically suffer from intrinsic anisotropies or large J_{1D} values, limiting the access to the full theoretical phase diagram. We report a comprehensive study of TLL and BEC phases in the organic Haldane chain system 3,5-bis(N-tert-butylaminoxy)-3'-nitro biphenyl (BoNO). The absence of anisotropy and a moderate J_{1D} enable exploration of the complete $B - T$ phase diagram. Through ^1H nuclear magnetic resonance, combined with theoretical analysis, we characterize the TLL properties, map the BEC phase boundary $T_c(B)$, determine the associated critical exponent $\nu \approx 0.66$ at B_{c2} , and demonstrate universal quasiparticle scaling in the quantum-critical regime. These results provide full experimental validation of theoretical predictions for field-induced phases in an $S = 1$ Haldane chain, made over two decades ago.

Quantum fluctuations determine the ground state properties of low-dimensional quantum magnets - networks of spins (S) forming chain or ladder structures - making them a compelling area of research. The relative simplicity of these systems allows for the development of theoretical models that can be directly and quantitatively compared to experimental results. This enables a deeper understanding of complex quantum phenomena they host, such as the Tomonaga-Luttinger liquid (TLL)¹ and a field-induced antiferromagnetic long range order (LRO) of Bose-Einstein condensate (BEC) type². The TLL theory provides a universal description of gapless systems with interacting quasiparticles in one dimension (1D). In the case of 1D spin systems, the low-energy excitation spectra can be modelled as quasiparticles with their properties fully determined by just two parameters: the renormalized Fermi velocity u and the dimensionless TLL interaction parameter K . At low temperatures, where the finite three-dimensional coupling (J_{3D}) between the 1D units comes into play, a 3D XY-AFM order emerges. This LRO can be viewed as the BEC state of a magnetic spin system that has been mapped onto a hard-core boson model. In both phases magnetic field acts as a chemical potential and can be used to modify the system's properties. The possibility to tune the system in a controlled manner makes simple 1D quantum magnets a perfect testing ground of theoretical predictions.

Arguably the most remarkable example of a spin chain is the $S = 1$ Haldane chain. More than 40 years ago Haldane discovered³ that a 1D system of integer spins described by the simple Heisenberg antiferromagnetic ($J_{1D} > 0$) Hamiltonian $H_0 = J_{1D}\sum_{ij}\mathbf{S}_i\mathbf{S}_j$ hosts a non-magnetic singlet ground state separated by an energy gap Δ from the first excited triplet state. This contrasts the half-integer spin chains where the ground state is gapless, and implies that Δ emerges from a distinct quantum nature of the system. The ground state, called the Haldane phase, remains stable^{4,5} in the presence of a relatively small single-ion anisotropy (D) and finite J_{3D} , inevitable in any real material. However, when the $S = 1$ chain is placed in an external magnetic field (B), the Zeeman splitting lowers the energy of the $S_z = +1$ triplet band and closes the gap at $B_{c1} = \Delta/g\mu_B$ (Fig. 1). Therefore, the B_{c1} is a quantum-critical point (QCP) as quantum fluctuations drive the ground state transition at $T = 0$ K. For $B \geq B_{c1}$, the excitation spectrum is gapless and for $T \leq J_{1D}$ the TLL state with attractive interactions emerges. The TLL parameter K can be tuned by further increase in B , as the fermion band is filled. In the presence of J_{3D} interactions, a 3D long-range ordered BEC state forms below $T_c(J_{3D})$. These gapless phases persist up to $B_{c2} \approx 4J_{1D}/g\mu_B$, at which the system reaches a complete polarization and the spectrum again becomes gapped. Such a rich phase diagram motivated an extensive research

of the Haldane chains and, so far, more than a dozen compounds have been synthesized in which a Haldane phase ground state is realized⁶. Remarkably, none of the systems were suitable for a comprehensive study of the field induced phases across the complete $B - T$ phase diagram (see Table S1). In the majority of systems, the $S = 1$ resides on a transition-metal ion, e.g. Ni^{2+} ion in CsNiCl_3 , $\text{Ni}(\text{C}_5\text{D}_{14}\text{N}_2)_2\text{N}_3\text{PF}_6$ (NDMAP), $\text{Ni}(\text{C}_2\text{H}_8\text{N}_2)_2\text{NO}_2\text{ClO}_4$ (NENP) and $\text{Ni}(\text{C}_3\text{H}_{10}\text{N}_2)_2\text{NO}_2\text{ClO}_4$ (NINO), where the inherent spin-orbit coupling introduces additional terms to the Hamiltonian, breaking the $U(1)$ symmetry necessary for a BEC state to form. For example, in NENP, NINO and NDMAP, a magnetic field oriented along the chain direction creates a staggered component of the field, because the principal axes of the g -tensor (at two Ni sites) are tilted by a certain angle $\pm\theta$ which cannot be compensated by rotating the sample. NINO and NENP also have a finite axial (D) and rhombic (E) single-ion anisotropy terms, and CsNiCl_3 orders at zero magnetic field. In addition, in many systems J_{1D} was too large to reach B_{c2} , or even B_{c1} . Consequently, the long-standing theoretical predictions on the properties of TLL^{7,8} or BEC^{9,10} phases in a model Haldane chain have yet to be confirmed.

Recently, a different route to the design of Haldane $S = 1$ chains has been taken¹¹. The newly synthesized nitroxide radical-based system 3,5-bis(N-tert-butylaminoxy)-3'-nitrobiphenyl (*m*-NO₂PhBNO, abbreviated as BoNO) is fully organic, with the $S = 1$ units made of two ferromagnetically coupled ($|J_{FM}| \gtrsim 500$ K) unpaired electrons from aminoxy groups. The delocalized character of the spin density (see Fig. S1) results in a negligible spin-orbit coupling, thus preserving the symmetry of the spin Hamiltonian. BoNO crystallizes in an orthorhombic *Pbca* unit cell with chains running along the crystallographic *a* axis, where $z = 6$ neighbouring chains form a distorted hexagonal lattice (Fig. S2). The remarkably low anisotropy manifests in an almost isotropic electron g tensor in the paramagnetic state, with $g_a = 2.0041$, $g_b = 2.0065$, and $g_c = 2.0063$ close to the free electron value of $g_e = 2.0023$.¹¹ The temperature dependence of low-field susceptibility $\chi(T)$ is almost identical along all three crystal axes and consistent with an antiferromagnetic $S = 1$ chain with an effective moment of $\mu_{\text{meas.}} = (2.7 \pm 0.1)\mu_B/\text{f.u.}$, intrachain coupling of $J_{1D} = (11.1 \pm 0.2)$ K and the total 3D coupling of $zJ_{3D} \approx 0.6$ K. Magnetization measurements at 1.3 K show a quasi-linear increase between $B_{c1} \approx 2$ T and $B_{c2} \approx 33$ T, compatible with coupled $S = 1$ chains with $zJ_{3D}/J_{1D} = 0.04$. BoNO is, therefore, a model Haldane chain system with critical field values that can be reached in a laboratory setting, which allows mapping of the field-induced phases in a complete $B - T$ phase diagram.

We present a ¹H nuclear magnetic resonance (NMR) study of magnetic-field induced phases and spin fluctu-

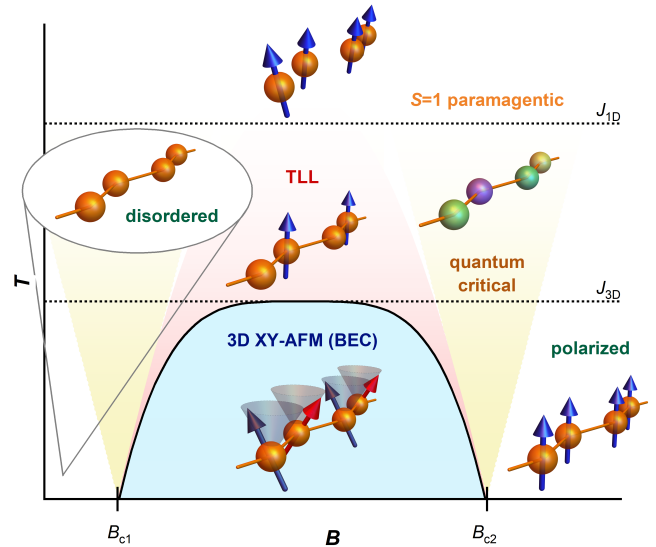


FIG. 1. The low-temperature phase diagram of a Haldane $S = 1$ chain in a magnetic field. In absence of the external magnetic field, a gap separates the singlet quantum-disordered (QD) ground state from the first excited triplet. The energy of the triplet is lowered via the Zeeman effect in a finite magnetic field, eventually closing the gap at B_{c1} . In the range $B_{c1} < B < B_{c2}$, the system is gapless and can be described by the TLL framework below energy scale set by J_{1D} . At lower temperatures, J_{3D} becomes relevant, and the system enters a long-range coherent 3D XY-AFM state, corresponding to the BEC in the bosonic mapping. Crossovers are indicated by dotted lines, while the solid line marks the phase transition. Universal quasiparticle behavior is observed in the quantum-critical (QC) region. At higher temperatures, system is an isotropic 3D $S = 1$ paramagnet.

ations in BoNO, in high magnetic fields (up to 34 T) and at temperatures down to 460 mK. To achieve this, we used an advanced NMR setup which allows measurements at high frequencies up to 1440 MHz. Our data reveal the long-sought evidence of attractive interactions across the TLL phase of a Haldane chain. Furthermore, we map out the field-induced BEC transition temperature $T_c(B)$ and show it defines a complete phase boundary of the BEC state by reproducing its shape via quantum Monte Carlo (QMC) calculations, and verifying the theoretical prediction $T_c(B) \propto (B - B_{c2})^\nu$ with $\nu = 2/3$ ¹² in the low- T limit close to B_{c2} . Our results are corroborated by magnetostriction measurements in pulsed magnetic fields, density matrix renormalization group (DMRG) calculation and extensive Bayesian inference analysis.

To investigate the properties of magnetic-field induced phases in BoNO for $B > B_{c1}$ we probe the electronic spin excitations via ¹H NMR. The typical ¹H spectrum of BoNO is defined by the Zeeman interaction via $f = {}^1\gamma(1 + \mathbf{K}_s)\mathbf{B}\mathbf{I}$, where ${}^1\gamma/2\pi = 42.5775$ MHz/T is the hydrogen gyromagnetic constant, \mathbf{B} is the magnetic field, \mathbf{I} nuclear spin, and \mathbf{K}_s the nuclear shift tensor.

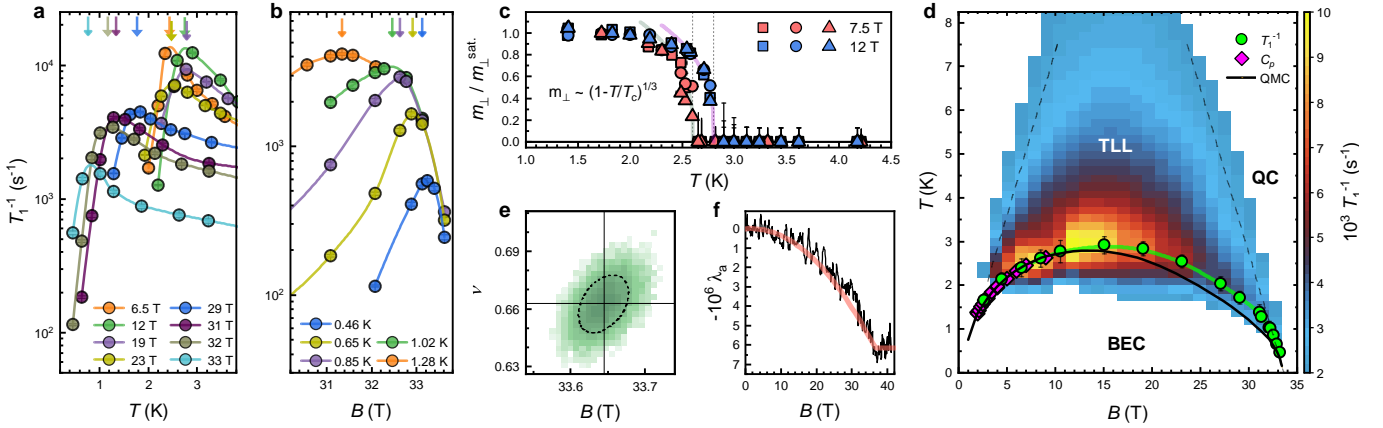


FIG. 2. Complete phase diagram of BoNO. **a** Temperature and **b** magnetic-field dependence of the ^1H relaxation rate T_1^{-1} across the phase transition at various external magnetic fields and temperatures, respectively. Solid lines are cubic-spline fits, and arrows mark the estimated transition temperatures $T_c(B)$. **c** Temperature evolution of the ordered transverse magnetic moment $m_\perp \propto \Delta f$ across T_c at 7.5 T (red) and 12 T (blue), determined from spectral splitting at various ^1H NMR lines (see Fig. S4). **d** Complete phase diagram derived from T_1^{-1} and spectral data (green circles). At low magnetic fields, additional heat-capacity measurements (magenta diamonds) corroborate the NMR-determined phase boundary. QMC simulations (black line) reproduce the experimental phase diagram perfectly up to 15 T, above which a small discrepancy develops, which can be reconciled by allowing for a field-dependent interchain coupling J_{3D} . **e** Probability density map of the upper critical field B_{c2} and critical exponent ν , calculated for $T_c \propto (B_{c2} - B)^\nu$ with the mean values of $B_{c2} = 33.645$ T and $\nu = 0.663$. Dashed line marks the 68% highest density interval (HDI). **f** Measured magnetostriiction along the chains $\lambda_a = (\Delta L_a / L_a)$ vs. B at 1.4 K shows a parabolic contraction up to B_{c2} . Red line is a guide to the eye.

The spectrum consists of a large number of spectral lines (Fig. S3) concentrated close to the bare nucleus Larmor frequency value $f_0 = {}^1\gamma B$ and several ^1H spectral lines shifted away from f_0 due to large hyperfine coupling $\mathbb{A} \propto K_s$ to electron magnetic moments. The shifted lines correspond to¹¹ the hydrogen sites H₁, H₃ and H₅ on the aromatic, electron-rich part of the BoNO molecule, making them very sensitive probes of the electronic dynamics. For an arbitrary magnetic field orientation one expects 4 spectral lines for each ^1H site, although due to the high crystal symmetry and significant spectral overlap fewer lines can be discerned.

Magnetic field-induced long range order. In Fig. 2a we show the relaxation rate $T_1^{-1}(T)$ dependence for various magnetic field values. Close to the saturation field, we did several isothermal $T_1^{-1}(B)$ measurements (Fig. 2b) at lowest temperatures. The data were collected on the isolated NMR line with the largest hyperfine shift to avoid spurious effects due to spectral line overlap (Fig. S3). The T_1^{-1} data probe the local electronic correlations in the low energy limit, making it a stringent probe of the system's ground state. For temperatures below 10 K ($\approx J_{1D}$), $T_1^{-1}(T)$ shows a slowly divergent behaviour as the system approaches the magnetic transition temperature T_c , where T_1^{-1} reaches a maximum value. Across T_c , the ^1H NMR spectra splits (Fig. 2c and Fig. S4) due to the onset of transverse magnetisation m_\perp . The line splitting Δf can be well described by the temperature dependence $(1 - T/T_c)^\beta$, with an exponent $\beta \sim 1/3$ fully consistent

with the 3D-XY universality class $\beta = 0.3485(2)$ ¹³. Below T_c , critical fluctuations increase and $T_1^{-1}(T)$ show a steep decrease, similar to other BEC systems^{14,15}. From the onset of splitting and the maximum in T_1^{-1} data, we determine the $T_c(B)$ phase boundary of the 3D LRO (Fig. 2d). The boundary $T_c(B)$ has a slightly asymmetric shape, with the maximum value of $T_c^{max.} = 2.9$ K at $B \approx 15$ T. The large $T_c^{max.}/J_{1D}$ value implies a significant interchain coupling zJ_{3D}/J_{1D} , in agreement with the $zJ_{3D}/J_{1D} \approx 0.06$ value estimated from the magnetic susceptibility measurements. At lower magnetic fields, hyperfine shifts are less pronounced, and the NMR spectra shrinks to the point where NMR lines start to overlap. Here, we have performed several specific heat capacity measurements down to 1.3 K to verify that $T_c(B)$ was correctly determined by NMR. Although the additional data provide a more detailed view of the phase boundary close to B_{c1} , as lower temperatures were not available, we estimate that B_{c1} value is $(1.0^{+0.5}_{-0.2})$ T. For the measurements at the high-field end, temperatures down to 460 mK were reached and we apply the low-temperature (LT) theoretical limit $T_c^{LT}(B) \propto |B - B_{c2}|^\nu$ to extrapolate $B_{c2} = (33.65 \pm 0.04)$ T and $\nu = (0.66 \pm 0.07)$ using a standard windowing¹⁸ method (Fig. S6) and Bayesian inference analysis (BIA) (Fig. 2e) (see Methods). BIA¹⁹ calculates conditional probabilities of observing specific values of parameters (B_{c2}, ν) for the given observed dataset $T_c(B)$ and in expectation of a well-defined functional dependence (here, $T_c^{LT}(B)$). It also pro-

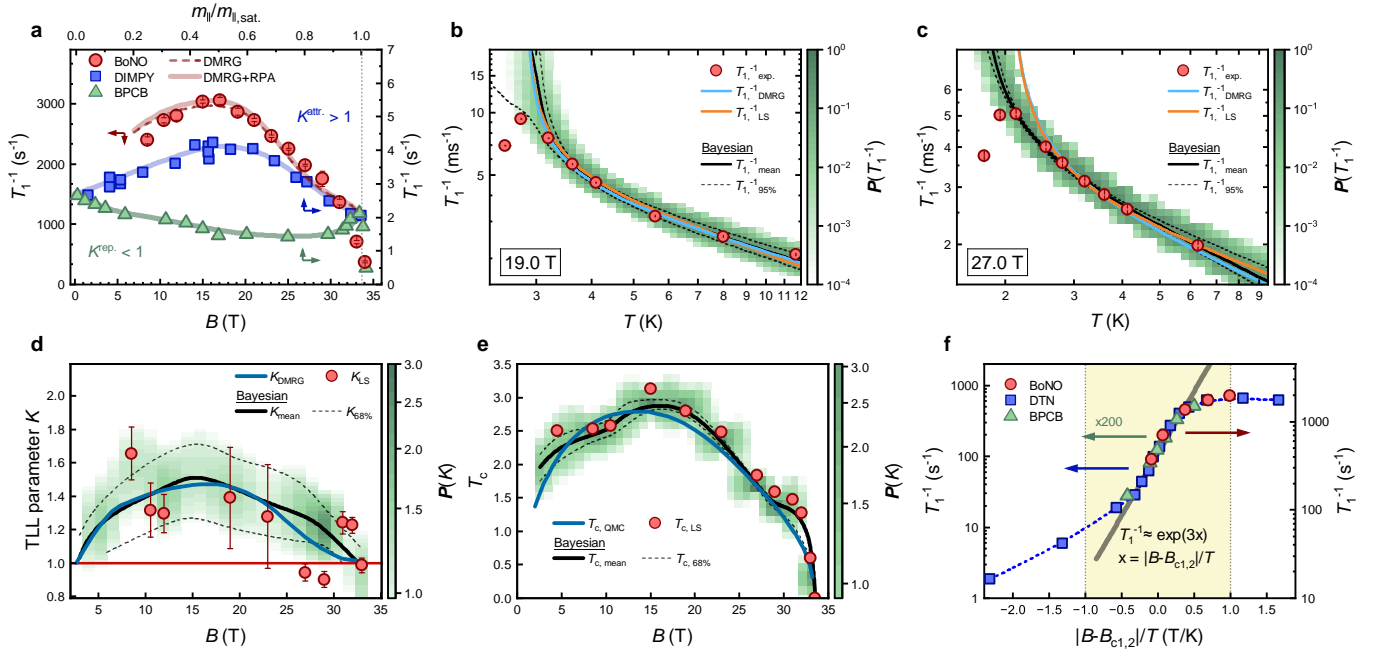


FIG. 3. Spin dynamics in Tomonaga–Luttinger and quantum-critical regimes. **a** Qualitative determination of the interaction parameter K from constant-temperature cuts of T_1^{-1} in the TLL regime (red circles), compared with DIMPY (blue squares) and BPCB (green triangles) from Ref. 16. The data predict attractive quasiparticle interactions ($K > 1$), as expected for the Haldane system. **b, c** Experimental $T_1^{-1}(T)$ data (red circles) overlaid with Bayesian probability distributions (green colormap) at 19 T and 27 T. Bayesian point estimates (mean and 95% HDI, black lines) are compared to the least-squares fits (LS, orange lines) and the theoretical $T_1^{-1}(T)$ dependence using DMRG data (blue lines). **d, e** Probability density maps (green) and point estimates (mean and 68% HDI, black lines) for K and T_c , compared with theory (blue lines) and LS fits (red circles). **f** Universal quasiparticle scaling of $T_1^{-1}(B)$ data measured across the quantum-critical region in BoNO (red circles), consistent with the three-magnon model (grey line), also observed¹⁷ in DTN (blue squares) and BPCB (green triangles).

vides point estimates and confidence intervals, and is more reliable in the case of limited or noisy datasets. The obtained exponent ν corresponds precisely to the universality class of a BEC quantum critical point, for which $\nu = z/D$ ^{12,20}, where $D = 3$ is the spatial dimensionality and $z = 2$ is the dynamical exponent associated with a quadratic triplon dispersion. With no anisotropy terms in the Hamiltonian, the upper critical field is then defined by a simple expression: $g\mu_B B_{c2} = 4J_{1D} + 2zJ_{3D}$. For consistency, using B_{c2} and J_{1D} we obtain $zJ_{3D} = 0.6 \pm 0.2$ K, in agreement with susceptibility and $B_{c1}(J_{3D})$ (as calculated by Ref. 5).

The phase boundary $T_c(B)$ is also calculated using the state-of-the-art quantum Monte Carlo (QMC) simulations. For simplicity, the calculation is done on an $S = 1$ chain with tetragonally coordinated J_{3D} . This does not affect the results as long as zJ_{3D} remains unaltered^{21,22}. Taking $zJ_{3D}^{\text{QMC}} = 0.676$ K, the calculated curve precisely follows the experimental data up to 10 T, with a small deviation for above 15 T. We present several options to address this discrepancy. One of them is the question of suitability of existing models. J_{3D} in BoNO is not isotropic - three different pairs of J_{3D} are distributed with a mirror symmetry along the ab plane. Specific geometry of these J_{3D} interactions may

modify the shape of $T_c(B)$ boundary. Unfortunately, this is not easy to take into account, since exact values of all J_{3D} interactions are difficult to determine, both theoretically and experimentally, and the introduced complexity makes numerical calculations unfeasible. The other cause of the discrepancy is the variation of J_{3D} and J_{1D} in the high-field region by magneto-elastic coupling. In a separate QMC calculation (see Supplementary Information F), we found that a 50% increase in the tetragonally symmetric J_{3D} can account for the experimental $T_c(B)$ boundary. Such a large variation is unusual and indicates that other parameters, e.g. J_{1D} , should also change. By a simple scaling we can estimate that an increase in J_{1D} up to 12% can also reproduce $T_c(B)$ data. Variations in the $zJ_{1D}(J_{3D})$ were observed in similar compounds^{23,24} where noticeable magnetostriction $\lambda_i = (\Delta L_i/L_i)$ ($i = a, b, c$) occurs. By measuring λ_a along the chain direction in pulse magnetic fields up to 41.2 T at 1.4 K, we detected a response of $-7 \cdot 10^{-6}$ (Fig. 2f), while $|\lambda_b|$ perpendicular to the chains was $\leq 8 \cdot 10^{-7}$, which is on the sensitivity limit of the method. While the exact evaluation of $zJ_{1D}(J_{3D})$ from the $\lambda_a(B)$ data is beyond the scope of this paper, we can conclude that variations of $J_{1D}(zJ_{3D})$ can account for the discrepancy.

Excitations of the 1D regime. In the TLL state of a strictly 1D system, we expect⁷ the transverse excitations originating at $q = \pi$ to be dominant, which results with a power-law²⁰ temperature dependence of the T_1^{-1} relaxation rate²⁵:

$$T_{1,\text{TLL}}^{-1} = \frac{\hbar\gamma^2 A_\perp^2 A_0^x}{k_B u} \cos\left(\frac{\pi}{4K}\right) B\left(\frac{1}{4K}, 1 - \frac{1}{2K}\right) \left(\frac{2\pi T}{u}\right)^{\frac{1}{2K}-1}, \quad (1)$$

where γ is the nuclear gyromagnetic ratio, A_\perp is the transverse hyperfine coupling constant, A_0^x is the amplitude of the spin correlation function, and $B(x, y) = \Gamma(x) \cdot \Gamma(y) / \Gamma(x + y)$. $K(B)$ dependence is defined by the properties of the original spin Hamiltonian. In the presence of sizeable 3D interactions ($zJ_{3D}/J_{1D} \gtrsim 0.01$) that increase T_c and reduce the span of the 1D regime, $T_1^{-1}(T)$ dependence is enhanced and warped²⁶⁻²⁸ by critical spin fluctuations. To account for the 3D effects and determine the correct K values, expression (1) should be modified: $T_1^{-1} = T_{1,\text{TLL}}^{-1} \Phi(K, T_c/T)$, where $\Phi(K, T_c/T)$ is an analytical correction factor based on random phase approximation (RPA) approach^{27,28}. We focus first on the isothermal $T_1^{-1}(B)$ dependence in the TLL regime. In the study of spin-ladder systems, it has been shown¹⁶ that far from T_c the $T_1^{-1}(B)$ dependence can reveal the nature of inherent fermionic interactions - a concave (convex) dependence directly reflects the attractive (repulsive) interactions in the system. The advantage of analysing $T_1^{-1}(B)$ is that it avoids possible ambiguities stemming from the delicate analysis of the $T_1^{-1}(T)$ data. It has long been theoretically predicted^{7,8} that for an $S = 1$ Haldane chain system the quasiparticle interactions in the TLL phase are attractive, and thus we expect a concave field dependence. In Fig. 3a we show the $T_1^{-1}(B)$ measured at 6.5 K ($> 2T_c^{\text{max.}}$) together with the previously reported data for the two ladder systems: $(\text{C}_7\text{H}_{10}\text{N})_2\text{CuBr}_4$ (DIMPY)¹⁶ and $(\text{C}_5\text{H}_{12}\text{N})_2\text{CuBr}_4$ (BPCB)²⁵, with attractive and repulsive interactions in the TLL regime, respectively. Clearly, BoNO displays attractive interactions of TLL quasiparticles. Apart from the qualitative behaviour, using the values of K , u , and A_0^x calculated by DMRG (see Supplementary Information G), we also quantitatively compare the experimental and numerical results, with A_\perp as a single fitting parameter. As shown, the calculated curves follow the experimental data, albeit for B close to B_{c1} and B_{c2} , where the system is close to the edges of the band, the TLL description is not suitable. It can also be seen that at this temperature the RPA correction only has a minor effect, which confirms the validity of our approach. Our data clearly reveal the presence of attractive interactions in the TLL state of a Haldane spin chain system in a broad region of phase space. This is the first direct demonstration of the theoretically predicted $K(B)$ dependence, made more than two decades ago.

We proceed to analyse our $T_1^{-1}(T)$ data by applying the least-square (LS) fitting of the complete expression

$T_1^{-1} = T_{1,\text{TLL}}^{-1} \Phi(K, T_c/T)$, with K and A_\perp as fitting parameters, and T_c determined from the experiment. Figures 3b and c (and Fig. S9) show an example of the fitted data at 19 T and 27 T. The resulting K_{LS} values dependence across the phase diagram are shown as red circles in Fig. 3d. Although the fitted K values are consistent with a dome-shaped DMRG predictions, the large parameter uncertainties are the result of scarce data points due to the limited measurement time on the high-field magnet. Curiously, the fitted $T_1^{-1}(T)$ curves are almost indistinguishable from the ones calculated using theoretical K values (Figs. 3b and c). Stability of LS fits depend on the number of measured points since the RPA correction function $\Phi(K, T_c/T)$ diverges at $T = T_c$, and the fitting procedure will dominantly minimize the square-error close to the divergence. We also treat our data using a BIA method (now with T_c as a fitting parameter) which compensates the mentioned issue and is well suited for this case¹⁹. In Figs. 3b and c we show the calculated probability distributions for the $T_1^{-1}(T)$ datasets, together with the mean values of the $T_1^{-1}(T)$ dependence and 95% HDI. In Figs. 3d and e we respectively show the resulting probability distribution for K parameter and T_c , with the mean values and 68% HDI. Our data show excellent agreement with theoretical predictions. This result serves as a consistency check of the $K(B)$ values obtained in the previous section and confirms the validity of the RPA-based correction^{27,28} to Haldane systems.

Quantum criticality. Finally, we focus on the $T_1^{-1}(B)$ data in the 1D regime for $B \approx B_{c2}$. With an increase of B for $T < J_{1D}$, the system crosses over from the gapless TLL into the gapped fully polarized phase through a quantum-critical region that expands in a characteristic V-shape²⁹ above 0 K to higher temperatures. For $B = B_{c2}$, where the system is directly at the QCP, one expects to find a universal and scale invariant¹⁷ T_1^{-1} dependence on $|B - B_{c1,c2}|/T$. Our data measured at 6.5 K are shown in Fig. 3f together with the data of the large- D spin $S = 1$ chain compound $\text{NiCl}_2\text{-4SC}(\text{NH}_2)_2$ (DTN) and the $S = 1/2$ ladder system BPCB from Ref. 17. Very close to B_{c2} , a steep $T_1^{-1}(B) \propto e^{-3\Delta(B)/T}$ dependence is observed, with $\Delta(B) = g\mu_B(B - B_{c2})/k_B$. The latter is driven by the critical excitations, theoretically described by three-magnon propagators³⁰ that have been shown to be very robust³¹ - perpetuating up to high temperatures. The scaled data for BoNO lie exactly on top of the other two systems, demonstrating the transition at B_{c2} is a true QCP. This perfect data overlap in three different systems shows that the universality is set by interaction-dependent scale factor, irrespective of the intrinsic nature of the system.

In summary, we presented an extensive study of the magnetic-field induced gapless phases in the new organic Haldane $S = 1$ chain $m\text{-NO}_2\text{PhBNO}$ (abbreviated as BoNO) across the $B - T$ phase diagram. The system is completely described by the quasi-1D Heisenberg Hamiltonian, without additional spin-orbit-related

terms, which means it can be used to study predictions of the pure Haldane chain system. Through the analysis of the TLL regime, we present the first confirmation of the theoretically predicted attractive interactions. At temperatures below 2.9 K, a long-range BEC-like order emerges, confirmed by the quantum Monte Carlo calculations, the critical exponent of $\nu = 0.66$ at B_{c2} and the quantum critical scaling that reveals a universally robust three-magnon spin-dynamics.

Methods

Samples. Single crystals of BoNO were grown using a synthesis process described in Ref. 11. Crystal structure and axes orientation was determined by a single-crystal X-ray diffraction using the Mo K α ($\lambda = 0.71$ Å) radiation source. For experiments we used a sample with dimensions $a \times b \times c = 2.7 \times 0.72 \times 0.1$ mm³.

Nuclear magnetic resonance. ¹H NMR measurements were performed using pulsed spectrometers. Data in magnetic fields up to 12 T were collected in an Oxford Instruments superconducting magnet in the NMR laboratory at University of Zagreb. Measurements at higher magnetic fields were performed in a 20 MW resistive magnet at high-magnetic field facility at LNCMI-CNRS in Grenoble. For the measurements up to 12 T the magnetic field was oriented parallel to the crystallographic *c* axis. Due to the overlap of NMR lines it was difficult to trace the lines when entering the ordered phase. Therefore, for the measurements in the resistive magnet, the sample was oriented away from the crystallographic axes so that we can keep track of each ¹H spectral line - the normalized magnetic field orientation was [0.373, 0.924, 0.077]. The spectra were collected by Hahn echo sequence $\pi/2 - \tau - \pi$ with a typical value of a $\pi/2$ pulse of 6 μ s, and $\tau = 100$ μ s. The T_1 measurements were performed using a saturation-recovery technique on a selected NMR line shown in Supplementary Fig. S3. Data were fitted to a magnetic relaxation function of the form: $M(t) = M_0(1 - e^{-(t/T_1)^\beta})$, where β was found to be ≈ 1 in all measurements.

Heat capacity. Heat capacity was measured using a home-made setup with a resistive heater attached to the sample by proton-free vacuum grease from Daikin Industries. The heater-sample assembly was mounted in vacuum and thermally isolated from the rest of the apparatus by a thin support wire. Heating was performed by applying current pulses to the resistor, and the temperature of the heater was simultaneously monitored through its resistance. From the deposited energy and the corresponding temperature change, the total heat capacity of the heater-sample system was obtained. To isolate the sample contribution, reference measurements were performed under identical conditions without the sample. Subtracting these data yielded the sample's heat capacity. The measurements were not calibrated to absolute units; thus, the reported heat capacity is given in arbitrary units. Nevertheless, this method is well suited to detecting phase transitions, since the heat capacity must

diverge at the transition temperature T_c for a second-order phase transition. Therefore, the T_c can be determined reliably even without an absolute calibration.

Magnetostriction. Magnetostriction measurements were performed in pulsed magnetic fields up to 41.2 T at the high-magnetic-field facility of HZDR in Dresden using the fiber Bragg grating (FBG) method³². Several samples with lengths of approximately 2–5 mm and a cross-section of 0.5×0.1 mm² were used. The samples were glued to an 80 μ m fiber using Loctite 401 cyanoacrylate, which has been shown to be safe for organic samples. The final data were averaged over three samples (a total of six measurements). The mechanical losses to the fiber were determined to be negligible, $(Y_{\text{fiber}} A_{\text{fiber}})/(Y_{\text{sample}} A_{\text{sample}}) < 3\%$.

Data analysis Quantitative analysis was carried out using a combination of least-squares (LS) fitting and Bayesian inference analysis (BIA). LS fitting minimizes the error function (χ^2) or maximizes the likelihood $p(x|\theta)$ of observing data x with the parameter vector θ in our hypothetical physical phenomena $f(x, \theta)$, yielding a single parameter vector θ as a point estimate. While straightforward, this approach is sensitive to noise and often converges only to local optima. BIA, by contrast, applies Bayes' theorem $p(\theta|x) \propto p(x|\theta)p(\theta)$ to generate a posterior probability distributions for the parameters. The question is now inverted - $p(\theta|x)$ tells us how likely we have parameters θ , given that we have just observed data x . This method provides both point estimates and confidence intervals, and is generally more robust when the dataset is limited or noisy, though results depend on the choice of prior distribution $p(\theta)$.

To facilitate numerical convergence in fitting T_1^{-1} , we first tabulated the multiplicative correction factor $\Phi(K, T_c/T)$ to the required precision²⁸. Bayesian sampling was performed with the PyMC5 library. The priors for K and T_c were set as truncated normal distributions centered at K_{DMRG} and T_c extracted from T_1^{-1} , respectively. The widths were chosen broad enough to avoid biasing the fits, with truncation ranges [0, 3] for K and [0, 10] K for T_c . The posterior distributions were constructed by drawing 5000 samples from 8 independent Markov chains. LS fitting used the same starting values but failed to converge at certain magnetic fields, in contrast to the Bayesian approach, which yielded stable posterior distributions and highest density ranges for all parameters.

DMRG and QMC data For one dimension, the TLL properties were computed using the density-matrix renormalization group (DMRG) method within the matrix product state formalism³³ based on ITensor library³⁴. Finite-temperature and thermodynamic properties of the three dimensional problem were obtained from quantum Monte Carlo simulations based on the stochastic series expansion algorithm with directed-loop updates³⁵. Large system sizes were simulated to access the thermodynamic limit, and statistical uncertainties were estimated from binning analysis after sufficient ther-

malization. A standard finite-size scaling analysis of the order parameter³⁶ was employed to extract the bulk 3D critical temperatures across the entire field range of the phase diagram shown in Fig. 2d.

Data availability statement

The datasets generated and/or analysed during the current study are available from the corresponding author on reasonable request.

REFERENCES

* corresponding author: mgribic.phy@pmf.hr

1. Giamarchi, T. *Quantum Physics in One Dimension* (Oxford University Press, 2003). URL <https://doi.org/10.1093/acprof:oso/9780198525004.001.0001>.
2. Zapf, V., Jaime, M. & Batista, C. D. Bose-Einstein condensation in quantum magnets. *Reviews of Modern Physics* **86**, 563–614 (2014). URL <https://link.aps.org/doi/10.1103/RevModPhys.86.563>.
3. Haldane, F. D. M. Nonlinear field theory of large-spin Heisenberg antiferromagnets: Semiclassically quantized solitons of the one-dimensional easy-axis Néel state. *Physical Review Letters* **50**, 1153–1156 (1983). URL <https://link.aps.org/doi/10.1103/PhysRevLett.50.1153>.
4. Sakai, T. & Takahashi, M. Effect of the Haldane gap on quasi-one-dimensional systems. *Physical Review B* **42**, 4537–4543 (1990). URL <https://link.aps.org/doi/10.1103/PhysRevB.42.4537>.
5. Wierschem, K. & Sengupta, P. Quenching the Haldane gap in spin-1 Heisenberg antiferromagnets. *Physical Review Letters* **112**, 247203 (2014). URL <https://link.aps.org/doi/10.1103/PhysRevLett.112.247203>.
6. Maximova, O. V., Streltsov, S. V. & Vasiliev, A. N. Long range ordered, dimerized, large-D and Haldane phases in spin 1 chain compounds. *Critical Reviews in Solid State and Materials Sciences* **46**, 371–383 (2021). URL <https://doi.org/10.1080/10408436.2020.1852911>.
7. Konik, R. M. & Fendley, P. Haldane-gapped spin chains as Luttinger liquids: Correlation functions at finite field. *Physical Review B* **66**, 144416 (2002). URL <https://link.aps.org/doi/10.1103/PhysRevB.66.144416>.
8. Fáth, G. Luttinger liquid behavior in spin chains with a magnetic field. *Physical Review B* **68**, 134445 (2003). URL <https://link.aps.org/doi/10.1103/PhysRevB.68.134445>.
9. Affleck, I. Theory of Haldane-gap antiferromagnets in applied fields. *Physical Review B* **41**, 6697–6702 (1990). URL <https://link.aps.org/doi/10.1103/PhysRevB.41.6697>.
10. Affleck, I. Bose condensation in quasi-one-dimensional antiferromagnets in strong fields. *Physical Review B* **43**, 3215–3222 (1991). URL <https://link.aps.org/doi/10.1103/PhysRevB.43.3215>.
11. Jakovac, I. *et al.* Properties of an organic model $S = 1$ Haldane chain system. *Physical Review B* **111**, 064407 (2025). URL <https://link.aps.org/doi/10.1103/PhysRevB.111.064407>.
12. Nikuni, T., Oshikawa, M., Oosawa, A. & Tanaka, H. Bose-Einstein condensation of dilute magnons in $TlCuCl_3$. *Physical Review Letters* **84**, 5868–5871 (2000). URL <https://link.aps.org/doi/10.1103/PhysRevLett.84.5868>.
13. Campostrini, M., Hasenbusch, M., Pelissetto, A., Rossi, P. & Vicari, E. Critical behavior of the three-dimensional XY universality class. *Physical Review B* **63**, 214503 (2001). URL <https://link.aps.org/doi/10.1103/PhysRevB.63.214503>.
14. Jeong, M. *et al.* Magnetic-order crossover in coupled spin ladders. *Physical Review Letters* **118**, 167206 (2017). URL <https://link.aps.org/doi/10.1103/PhysRevLett.118.167206>.
15. Blosser, D., Horvatić, M., Bewley, R., Gvasaliya, S. & Zheludev, A. Dynamics and field-induced order in the layered spin $S = 1/2$ dimer system $(C_5H_6N_2F_2)CuCl_4$. *Physical Review Materials* **3**, 074410 (2019). URL <https://link.aps.org/doi/10.1103/PhysRevMaterials.3.074410>.
16. Jeong, M. *et al.* Dichotomy between attractive and repulsive Tomonaga-Luttinger liquids in spin ladders. *Physical Review Letters* **117**, 106402 (2016). URL <https://link.aps.org/doi/10.1103/PhysRevLett.117.106402>.
17. Mukhopadhyay, S. *et al.* Quantum-critical spin dynamics in quasi-one-dimensional antiferromagnets. *Physical Review Letters* **109**, 177206 (2012). URL <https://link.aps.org/doi/10.1103/PhysRevLett.109.177206>.
18. Sebastian, S. E. *et al.* Characteristic Bose-Einstein condensation scaling close to a quantum critical point in $BaCuSi_2O_6$. *Physical Review B* **72**, 100404 (2005). URL <https://link.aps.org/doi/10.1103/PhysRevB.72.100404>.
19. von Toussaint, U. Bayesian inference in physics. *Rev. Mod. Phys.* **83**, 943–999 (2011). URL <https://link.aps.org/doi/10.1103/RevModPhys.83.943>.
20. Giamarchi, T. & Tsvelik, A. M. Coupled ladders in a magnetic field. *Physical Review B* **59**, 11398–11407 (1999). URL <https://link.aps.org/doi/10.1103/PhysRevB.59.11398>.
21. Sakai, T. & Takahashi, M. The ground state of quasi-one-dimensional Heisenberg antiferromagnets. *Journal of the Physical Society of Japan* **58**, 3131–3142 (1989). URL <https://doi.org/10.1143/JPSJ.58.3131>.
22. Wierschem, K. & Sengupta, P. Characterizing the Haldane phase in quasi-one-dimensional spin-1 Heisenberg antiferromagnets. *Modern Physics Letters B* **28**, 1430017 (2014).
23. Zapf, V. S. *et al.* Magnetostriiction in the bose-einstein condensate quantum magnet $NiCl_2\text{--}4SC(NH_2)_2$ (invited). *Journal of Applied Physics* **101**, 09E106 (2007). URL <https://doi.org/10.1063/1.2711612>.
24. Nomura, K. *et al.* Metastable magnetization plateaus in the $S=1$ organic spin ladder BIP-TENO induced by a microsecond-pulsed megagauss field. *Physical Review B* **105**, 214430 (2022). URL <https://link.aps.org/doi/10.1103/PhysRevB.105.214430>.
25. Klanjšek, M. *et al.* Controlling Luttinger liquid physics in spin ladders under a magnetic field. *Physical Review Letters* **101**, 137207 (2008). URL <https://link.aps.org/doi/10.1103/PhysRevLett.101.137207>.
26. Jeong, M. *et al.* Attractive Tomonaga-Luttinger liquid in a quantum spin ladder. *Physical Review Letters* **111**, 106404 (2013). URL <https://link.aps.org/doi/10.1103/PhysRevLett.111.106404>.

10.1103/PhysRevLett.111.106404.

27. Dupont, M., Capponi, S., Laflorencie, N. & Orignac, E. Dynamical response and dimensional crossover for spatially anisotropic antiferromagnets. *Physical Review B* **98**, 094403 (2018). URL <https://link.aps.org/doi/10.1103/PhysRevB.98.094403>.
28. Horvatić, M., Klanjšek, M. & Orignac, E. Direct determination of the Tomonaga-Luttinger parameter K in quasi-one-dimensional spin systems. *Physical Review B* **101**, 220406 (2020). URL <https://link.aps.org/doi/10.1103/PhysRevB.101.220406>.
29. Maeda, Y., Hotta, C. & Oshikawa, M. Universal temperature dependence of the magnetization of gapped spin chains. *Physical Review Letters* **99**, 057205 (2007). URL <https://link.aps.org/doi/10.1103/PhysRevLett.99.057205>.
30. Orignac, E., Citro, R. & Giamarchi, T. Critical properties and Bose-Einstein condensation in dimer spin systems. *Physical Review B* **75**, 140403 (2007). URL <https://link.aps.org/doi/10.1103/PhysRevB.75.140403>.
31. Ranjith, K. M., Landolt, F., Raymond, S., Zheludev, A. & Horvatić, M. NMR evidence against a spin-nematic nature of the presaturation phase in the frustrated magnet $\text{SrZnVO}(\text{PO}_4)_2$. *Physical Review B* **105**, 134429 (2022). URL <https://link.aps.org/doi/10.1103/PhysRevB.105.134429>.
32. Daou, R. *et al.* High resolution magnetostriction measurements in pulsed magnetic fields using fiber Bragg gratings. *Review of Scientific Instruments* **81**, 033909 (2010). URL <https://doi.org/10.1063/1.3356980>.
33. Schollwöck, U. The density-matrix renormalization group in the age of matrix product states. *Annals of Physics* **326**, 96–192 (2011). URL <https://www.sciencedirect.com/science/article/pii/S0003491610001752>. January 2011 Special Issue.
34. Fishman, M., White, S. R. & Stoudenmire, E. M. The ITensor Software Library for Tensor Network Calculations. *SciPost Physics Codebases* 4 (2022). URL <https://scipost.org/10.21468/SciPostPhysCodeb.4>.
35. Syljuåsen, O. F. & Sandvik, A. W. Quantum Monte Carlo with directed loops. *Physical Review E* **66**, 046701 (2002). URL <https://link.aps.org/doi/10.1103/PhysRevE.66.046701>.
36. Sandvik, A. W. Computational studies of quantum spin systems. *AIP Conference Proceedings* **1297**, 135–338 (2010). URL <https://doi.org/10.1063/1.3518900>.

Acknowledgments We acknowledge fruitful discussions with P. Sengupta. M.S.G. and I.J. acknowledge the support of Croatian Science Foundation (HRZZ) under the project IP-2018-01-2970 and the support of project CeNIKS co-financed by the Croatian Government and the European Union through the European Regional Development Fund - Competitiveness and Cohesion Operational Programme (Grant No. KK.01.1.1.02.0013). M.D. completed his contribution to this work prior to joining Rigetti Computing. We acknowledge the support of LNCMI-CNRS and HLD-HZDR, members of the European Magnetic Field Laboratory (EMFL).

Author contributions M.S.G., I.J., M.H., M.T. and S.K. performed NMR experiments and the data analysis. I.J., Y.S. and S.L. performed magnetostriction measurements. M.S.G. and I.J. wrote the paper. M.S.G. conceived the project and planned the research. Y.H. synthesized the samples. M.D., N.L. and S.C. performed QMC and DMRG calculations. All authors took part in discussing results, contributed to data interpretation and editing the manuscript.

Correspondence and requests for materials should be addressed to M.S.G.

Competing interests The authors declare no competing interests.